CrossMark

Effect of Isothermal Heating Temperature on the Interfacial Reactions Between Fe-Al-Ca Alloy and Al₂O₃-CaO-FeO Oxide

CHENGSONG LIU [ORCID],[1,2,4] HUA ZHANG,[1,5] XIAOQIN LIU,[3] and FEI YE[1]

1.—The State Key Laboratory of Refractories and Metallurgy, Wuhan University of Science and Technology, Wuhan 430081, People's Republic of China. 2.—Department of Materials Science and Engineering, Carnegie Mellon University, Pittsburgh, PA 15213, USA. 3.—Engineering Training Center, Wuhan University of Science and Technology, Wuhan 430081, People's Republic of China. 4.—e-mail: chengsol@andrew.cmu.edu. 5.—e-mail: huazhang@wust.edu.cn

To further investigate the effects of isothermal heating temperature on the interfacial reactions between the Fe-Al-Ca alloy and the Al₂O₃-CaO-FeO oxide, two kinds of diffusion couples with different FeO contents in the oxide were prepared and then subjected to isothermal heating at different temperatures in the range of 873 K to 1473 K for 10 h, 30 h, and 50 h. With increasing temperature of isothermal heating, in the case of 0.5 mass% FeO, fine Al₂O₃ particles first precipitated in the alloy near the alloy–oxide interface, and then CaO·Al₂O₃ branch inclusions appeared and increased in number, while for the case of 3.0 mass% FeO, Al₂O₃ particles were the only reaction product in the particle precipitation zone (PPZ). An improved kinetics model for predicting PPZ width was proposed and verified by experimental results.

INTRODUCTION

In general, nonmetallic inclusions have detrimental effects on the mechanical properties of steels.[1] To modify the physicochemical characteristics of nonmetallic inclusions in molten steel, various operating measures, including deoxidation, optimization on the refining slag composition, calcium treatment, rare earth treatment, and so on, have been introduced into the steelmaking process and continuously improved.[2,3] However, it has been found that the composition, morphology, size, and distribution of inclusions in the final steel product are sometimes different from those in the molten steel due to the reactions between the steel and inclusions during heat treatment. Takahashi et al.[4] found that by heating at 1373 K for 1 h, the SiO₂ and Cr₂O₃ contents of MnO-SiO₂-type inclusions in the stainless steel could gradually decrease and increase, respectively. This phenomenon would not occur after the heating at 1573 K for 1 h. H. Shibata et al.[5] concluded that the critical Si content in the steel where the stable inclusion changed from MnO-SiO₂ to MnO-Cr₂O₃ was approximately 0.3 mass% for 10 mass% Cr steel after the heat treatment at

1473 K. Ren et al.[6] studied the transformation of oxide inclusions in type 304 stainless steels during heat treatment and found that elemental Cr in the steel could react with manganese silicate to form spinel during the heating at the range of 1273 K to 1473 K. Many previous studies indicate heat treatment gradually becomes a new approach for precisely controlling the physicochemical characteristics of nonmetallic inclusions in steel.[7–11]

Al₂O₃ is one of the most common deoxidization products that can be typically modified by calcium treatment to avoid possible steel defects, such as stress cracks, surface inclusions, and clogging of the submerged entry nozzle during continuous casting, by forming calcium aluminate with low hardness and a low melting temperature.[12] The formation, floatation, and removal of calcium aluminates in molten steel during steelmaking processes at high temperatures have been widely studied.[13–15] However, less attention has been paid to the evolution of calcium aluminates in solid steel during heat treatment since little change is commonly deemed to occur. In our previous work,[16] it was found that the equilibrium oxide with Fe-Al-Ca alloy at 1873 K is not a binary oxide of Al₂O₃-CaO but a ternary

compound of Al_2O_3, CaO, and 0.5 mass% FeO. Solid-state reactions actually have been confirmed between the Fe-Al-Ca alloy and the Al_2O_3-CaO-FeO oxide during the heating at 1473 K, which are originally equilibrated at 1873 K. Al_2O_3 particles and $CaO \cdot Al_2O_3$ branch inclusions with high hardness and high melting temperatures precipitated as reaction products in the alloy near the alloy–oxide interface. Furthermore, due to the nonequilibrium among molten steel, inclusions, and partial oxygen pressure in the system, FeO content in the inclusions might be higher than the equilibrium value in the molten steel at 1873 K. As the initial FeO content in the oxide increased, the $CaO \cdot Al_2O_3$ branch inclusions gradually disappeared from the particle precipitation zone (PPZ) where Al_2O_3 particles form.[17] However, in the previous studies, the effects of isothermal heating temperature and time on the interfacial reactions between the Fe-Al-Ca alloy and the Al_2O_3-CaO-FeO oxide and their evolution mechanism were not fully clarified, and these effects are of great importance in the subsequent hot rolling and heat treatment processes, especially for diffusion annealing with high temperature and long heat-treated time.

In this study, two kinds of diffusion couples with different FeO contents in the Al_2O_3-CaO-FeO oxides were produced and then subjected to isothermal heating at different temperatures in the range of 873 K to 1473 K for 10 h, 30 h, and 50 h. The effects of isothermal heating temperature on the interfacial reactions between the Fe-Al-Ca alloy and the Al_2O_3-CaO-FeO oxide were further revealed and discussed. An improved kinetics model was established to predict the PPZ width in the alloy at the alloy–oxide interface during the heating process and subsequently verified by the experimental results.

EXPERIMENTAL PROCEDURE

Preparation of the As-Cast Alloy and Oxides

Table I shows the initial composition of the Fe-Al-Ca alloy and the Al_2O_3-CaO-FeO oxide used in the isothermal heating experiments. Diffusion couples A and B contain 0.5 mass% and 3.0 mass% of FeO, respectively. High-purity electrolytic iron, aluminum, and calcium were melted at 1873 K for 0.5 h using a vacuum induction furnace to fabricate the Fe-Al-Ca alloy with very few inclusions. When

the vacuum degree reached 10^{-2} torr, high-purity argon gas (99.9 mass%) was introduced to fill the chamber to a pressure of 1 atm. To prepare the Al_2O_3-CaO-FeO oxide, reagent grade Al_2O_3 (purity 99.6 mass%), CaO (purity > 99 mass%), and FeO (purity > 99 mass%) were fully mixed. The mixture was then put into a platinum crucible containing a lid and inserted into an electric resistance furnace. It was melted in the furnace at 1973 K and homogenized for 0.5 h, and then it was withdrawn from the furnace and rapidly cooled in an argon stream. Powders were machined from the Fe-Al-Ca alloy to measure contents of the total calcium (T. Ca), the dissolved aluminum ($[Al]_s$), and the total sulfur (T.S.) in the alloy. A 5-mm-diameter rod was machined from the sample to test T.O. content. The chemical compositions of the bulk alloy and Al_2O_3-CaO-FeO oxide were determined by inductively coupled plasma optical emission spectrometry (ICP-OES).

Oxide Premelting, Vacuum Sealing, and Isothermal Heating Experiments

To simulate the state of the inclusions in the alloy, good contact between the Fe-Al-Ca alloy and the Al_2O_3-CaO-FeO oxide was necessary. In this study, confocal scanning laser microscopy (CSLM) was employed to melt the oxide and produce diffusion couples. On the surface of the alloy sample ($\Phi 5.0 \times 3.0$ mm), a small circular hole (about $\Phi 1.5$ mm, depth: 2.0 mm) was formed to support the oxide power. The alloy and oxide were then put into an Al_2O_3 crucible (O.D. 9 mm, I.D. 8 mm, height 3.5 mm), and a piece of Ti foil was set around the crucible to further lower the oxygen partial pressure at high temperature. After the overall pressure in the chamber of the CSLM instrument reached 5.0×10^{-3} Pa, high-purity argon gas was introduced to keep the alloy samples from oxidation. The temperature rose from room temperature to 1700 K (about 20 K higher than the melting temperature of the oxide). Once the oxide melted, the sample was immediately quenched in a helium stream. The heating and cooling rates were approximately 100 K/min and 1000 K/min, respectively.

Subsequently, each specimen along with a piece of Ti foil and two blocks of alloy of the same composition was sealed in a quartz tube filled with pure argon gas after the oxide premelting process. By

Table I. Initial compositions of the Fe-Al-Ca Alloy and Al_2O_3-CaO-FeO oxide used in the isothermal heating experiments

Diffusion couple	Alloy (mass%)					Oxide (mass%)		
	Fe	$[Al]_s$	T.Ca	T.S.	T.O.	Al_2O_3	CaO	FeO
A	Bal.	0.4	0.004	0.003	0.0015	51.26	48.24	0.50
B						50	47	3.0

Effect of Isothermal Heating Temperature on the Interfacial Reactions Between Fe-Al-Ca Alloy and Al_2O_3-CaO-FeO Oxide

1795

vacuum pumping, the quartz tube was first evacuated to 1.0×10^{-2} Pa and then high-purity argon gas was introduced to fill the tube to a pressure of 2×10^4 Pa. The quartz tube was subsequently heat-treated in a high-temperature tube furnace and then quenched with water. Here, A1-x, A2-x, A3-x, and A4-x are the samples with 0.5 mass% FeO in the alloy obtained after isothermal heating at 873 K, 1073 K, 1273 K, and 1473 K for x h, respectively, where x = 10, 30, or 50, indicating the time length of isothermal heating. The samples B1-x, B2-x, B3-x, and B4-x contain 3.0 mass% FeO in the alloy and were obtained after isothermal heating at 873 K, 1073 K, 1273 K, and 1473 K for x h, respectively.

Sample Characterization Method

The compositions and phases of the Fe-Al-Ca alloy and the Al_2O_3-CaO-FeO oxide at each alloy–oxide interface after the isothermal heating were then measured and analyzed by electron probe x-ray microanalysis (EPMA) after the samples grinded by SiC sand papers and polished with diamond paste. To reduce the error, the elements in the alloy were calibrated using standard samples before every analysis. The mass fractions of Al_2O_3, CaO, and FeO were obtained by direct conversion from the determined contents of Al, Ca, and Fe, respectively, in the oxide. The area proportions of the phases in the alloy and the oxide after isothermal heating were measured by an ASPEX automatic scanning electron microscope.

RESULTS

It was found that the experiments after the heat treatment for 10 h, 30 h, and 50 h presented similar results, and the extent of reactions varied with the heating time. Here, to clearly display the reaction phenomena between the Fe-Al-Ca alloy and the Al_2O_3-CaO-FeO oxide, experiment results after the isothermal heating for 50 h are typically exhibited and analyzed.

Figure 1 shows the interfaces between the alloy and the oxide in the diffusion couples A1-50, A2-50, A3-50, A4-50, B1-50, B2-50, B3-50, and B4-50 after heat treatment for 50 h. It is observed that after heating at 1700 K, good contact was obtained between the Fe-Al-Ca alloy and the Al_2O_3-CaO-FeO oxide in each specimen. As shown in Fig. 1a, after isothermal heating at 873 K for 50 h, gray Al_2O_3 particles precipitated in the alloy near the alloy–oxide interface. As the heating temperature increased to 1073 K, strip $CaO·Al_2O_3$ inclusions appeared and developed in Fig. 1b. Some white iron particles precipitated in the Al_2O_3-CaO-FeO oxide. When the heating temperature reached 1273 K and 1473 K, as shown in Fig. 1c and d, the morphology of the $CaO·Al_2O_3$ inclusions changed from strips to branches. Several phases, including a main gray $12CaO·7Al_2O_3$ phase and white iron particles, were also observed in the oxide. In addition, the quantities and scales of the precipitated Al_2O_3 particles and $CaO·Al_2O_3$ inclusions in the alloy and iron particles in the oxide were positively correlated with the isothermal heating temperature. Figure 1e–h demonstrates that for an initial FeO content in the Al_2O_3-CaO-FeO oxide of 3 mass%, only gray Al_2O_3 particles precipitated in the Fe-Al-Ca alloy near the alloy–oxide interface after isothermal heating for 50 h. Furthermore, the gray Al_2O_3 particles at the precipitation front were larger than those near the alloy–oxide interface, as shown in Fig. 1f. This phenomenon became even more obvious with increasing isothermal heating temperature, as shown in Fig. 1g and h. The morphology and compositions of the phases in the oxide were similar to those in the diffusion couples A1-50, A2-50, A3-50, and A4-50. However, the quantities and sizes of the white iron particles became larger.

Figure 2 shows the compositions of the alloy and oxide near the interfaces of the diffusion couples A1-50, A2-50, A3-50, A4-50, B1-50, B2-50, B3-50, and B4-50. As the X axis, "Distance from the interface" represents the perpendicular distance between the analysis point and the alloy–oxide interface. Composition analysis directions in the alloy and oxide are shown in Fig. 1a as an example. The same analysis method has been employed on the other samples hereafter. After isothermal heating for 50 h, the Al concentration in the alloy near the alloy–oxide interfaces decreased from an initial value of 0.4 mass% to approximately 0.02 mass%, while the Ca concentration increased from an initial value of 0.004 mass% to approximately 0.26 mass% in diffusion couples A and B, as shown in Fig. 2a–d. In this study, the region with a lower Al content than that in the bulk alloy is defined as the Al-depleted zone (ADZ). Similarly, the region with a higher Ca content than that in the bulk alloy is defined as the Ca-accumulated zone (CAZ). It is thought that the precipitation of fine Al_2O_3 particles results in the variation of Al concentration in the alloy near the alloy–oxide interface, while it affects the Ca concentration little. The ADZ width exhibited a significantly positive correlation to the isothermal heating temperature, whereas the CAZ width was quite stable in all cases. Compared with the initial composition of bulk oxide shown in Table I, as for diffusion couples A after isothermal heating, the Al_2O_3 and CaO contents in the oxide close to the alloy–oxide interface shown in Fig. 1e were higher and lesser than the initial ones in bulk oxide, respectively. However, this phenomenon did not occur in diffusion couples B where after isothermal heating the Al_2O_3 and CaO contents in the oxide close to the alloy–oxide interface were almost the same as those in the bulk oxide, as shown in Fig. 1f. In all cases after isothermal heating for 50 h, the FeO content in whole bulk oxide decreased and its decreasing range had a positive correlation with the heating temperature, as shown in Fig. 2g
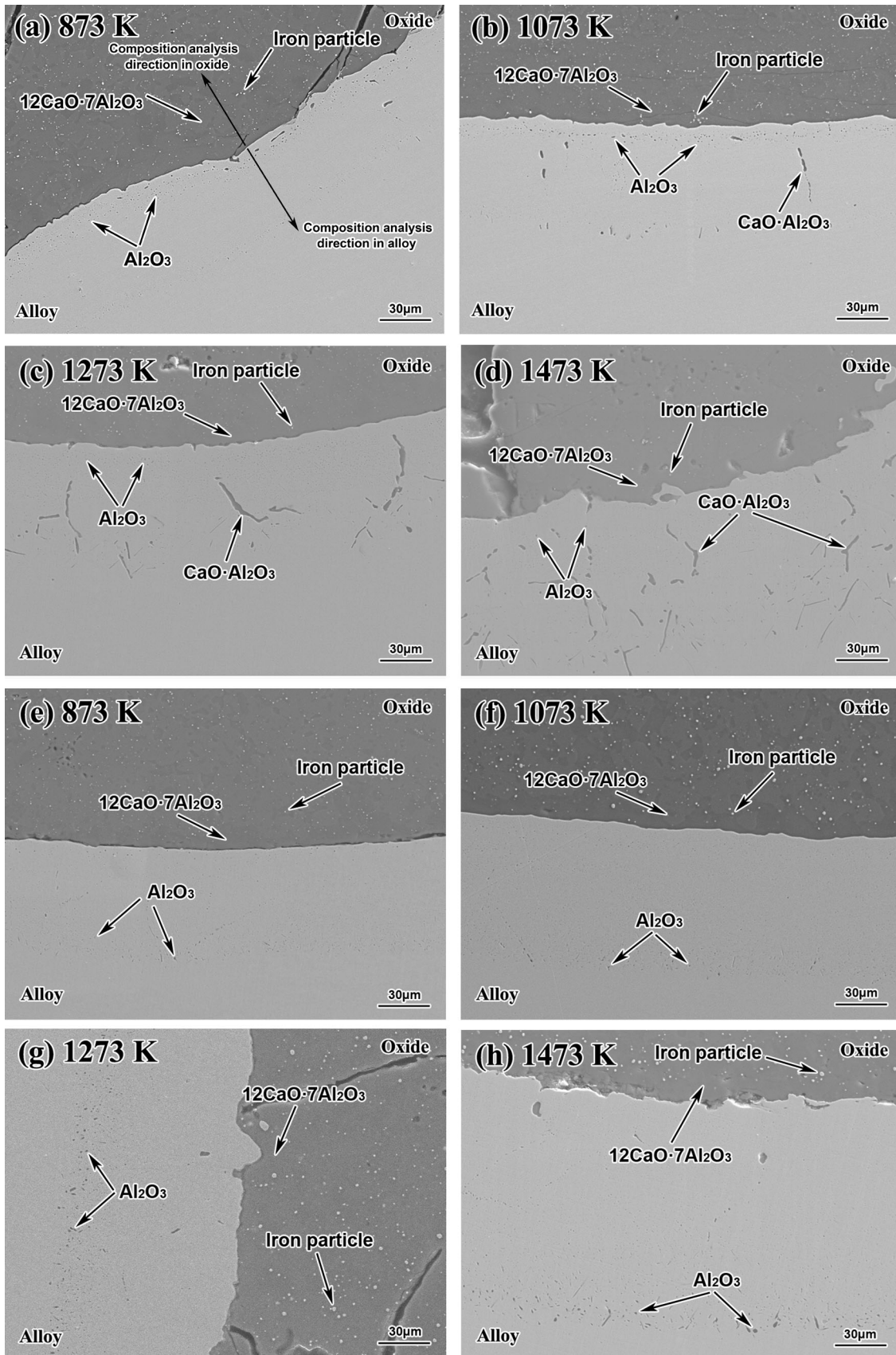
Fig. 1. Interfaces between the alloy and the oxide in the diffusion couples (a) A1-50, (b) A2-50, (c) A3-50, (d) A4-50, (e) B1-50, (f) B2-50, (g) B3-50, and (h) B4-50 after isothermal heating for 50 h.

and h. It is expected that the quantities and sizes of the white iron particles that precipitated in the Al_2O_3-CaO-FeO oxide also increased with the decrease of the FeO content due to its separation according to the experimental results.
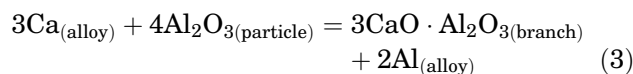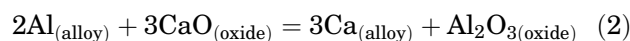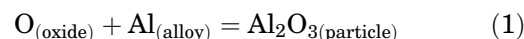
Figure 3 shows the compositions of the alloy and oxide near the interfaces of the diffusion couples A and B before and after isothermal heating at 1473 K for 10 h, 30 h, and 50 h. After heating, in diffusion couples A, as shown in Fig. 3a and c, the Al concentration in the alloy near the alloy–oxide interfaces decreased from an initial value of 0.4 mass% to approximately 0 mass%, while the Ca concentration increased from an initial value of 0.004 mass% to approximately 0.28 mass%. With increasing isothermal heating time, the ADZ width increased and the CAZ width remained at approximately 20 μm in all cases. Similar influences of the isothermal heating time on the Al and Ca contents in the alloy, the ADZ and CAZ widths in diffusion couples B were also confirmed, as shown in Fig. 1b and d. As for the composition of the oxide shown in Fig. 3e–h, the Al_2O_3 and CaO contents in the oxide close to the alloy–oxide interface and FeO content in the whole oxide in diffusion couples A and B have the same trend as those in Fig. 2. In addition, it is also confirmed that increasing the range of Al content and decreasing the range of Ca content near the alloy–oxide interface, as well as decreasing the range of FeO content in the oxide, all have positive correlations with the heating time.

DISCUSSION

Mechanism of the Interfacial Reactions

In this study, the experimental results after isothermal heating for 50 h suggested that for the low initial FeO content of the oxide (0.5 mass%) in diffusion couple A, the amount of Al_2O_3 particles and CaO·Al_2O_3 branch inclusions that precipitated in the alloy near the alloy–oxide interface increased with increasing temperature from 873 K to 1473 K. For the initial FeO content of the oxide of 3.0 mass%, only Al_2O_3 particles precipitated as the reaction product in the alloy near the alloy–oxide interface, while CaO·Al_2O_3 branch inclusions were not observed. It is inferred that the precipitation reaction for Al_2O_3 particles, as shown in Eq. 1, occurs prior to the generation of CaO·Al_2O_3 branch inclusions when the initial FeO content in the oxide is higher (3.0 mass%). As the FeO content decreased to some extent during the isothermal heating, CaO·Al_2O_3 branch inclusions were observed.[16,17] It is thought that during isothermal heating, the FeO in the oxide gradually separates into iron and elemental O. The excess oxygen diffuses from the Al_2O_3-CaO-FeO oxide to the Fe-Al-Ca alloy and reacts with the elemental Al in the alloy to generate Al_2O_3 particles. Furthermore, the reduction of CaO has been reported to result in unintended changes to characteristics of inclusions, as shown in Eq. 2.[18]

According to the experimental results shown in Figs. 2 and 3, it was inferred that during isothermal heating, in diffusion couples A, elemental Al in the alloy would also react with the CaO in the oxide resulting in the increase of Ca content in the alloy and the increase of Al_2O_3 content in the oxide close to the alloy–oxide interface. Thus, the reaction for the formation of CaO·Al_2O_3 branch inclusions can be expressed by Eq. 3. Due to the lack of thermodynamic data for these solid-state reactions, the basic thermodynamic data at 1873 K were extended to a lower temperature for approximate calculation. In Eq. 3, the elemental Ca in the alloy was mainly supplied from the CaO in the oxide by Eq. 2. Activities of Al_2O_3 particle and CaO·Al_2O_3 branch inclusions in the alloy are both unity. Thus, the formation of CaO·Al_2O_3 branch inclusions is thermodynamically feasible.

$$O_{(oxide)} + Al_{(alloy)} = Al_2O_{3(particle)} \tag{1}$$

$$2Al_{(alloy)} + 3CaO_{(oxide)} = 3Ca_{(alloy)} + Al_2O_{3(oxide)} \tag{2}$$

$$3Ca_{(alloy)} + 4Al_2O_{3(particle)} = 3CaO \cdot Al_2O_{3(branch)} + 2Al_{(alloy)} \tag{3}$$

Modified Kinetics Calculation Model

In this study, the reactions between the alloy and the oxide were similar to that of internal oxidation since the formation of an external oxidation layer, i.e., a scale, was not observed. The kinetics of internal oxidation has been investigated by a number of researchers.[19–23] Bohm et al.[20] investigated the internal oxidation of metallic alloys and established a function relationship between the number of oxide particles precipitating per unit volume with the experimental conditions and the distance from the phase boundary and then verified it by experiments on Ag-Cd alloys. In our previous work,[21,22] interfacial reactions between MnO-SiO_2-FeO oxide and Fe-Mn-Si alloy and the effect of FeO and sulfur on the reactions were studied. The widths of the PPZ and MDZ (Mn-depleted zone) increased with heat treatment time and decreased with the increasing sulfur content of oxide. The distances of oxygen diffusion in the experiments were successfully estimated by Wagner's equation,[19] with FeO content in the oxide. In this study, the method used to define and calculate the PPZ width in the experiments was shown in Fig. 4, wherein more than two inclusions are counted in a rectangle area of 50 μm parallel to the interface and 5 μm perpendicular to the interface.

The separation and reduction of FeO in the Al_2O_3-CaO-FeO oxide, as the oxygen supplier, generally determined the PPZ width in the Fe-Al-Ca alloy near the alloy–oxide interface. Thus, to establish a dynamic model for theoretically calculating the PPZ
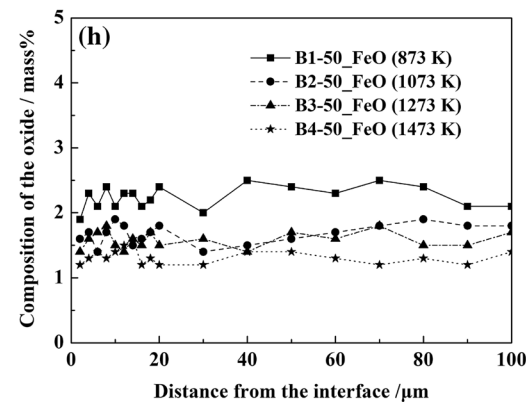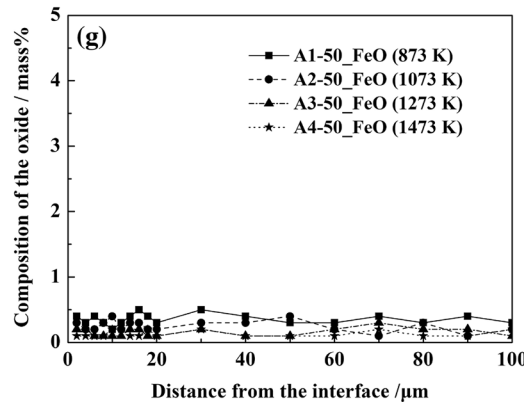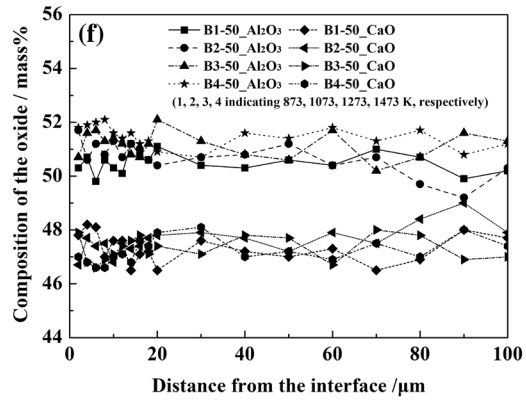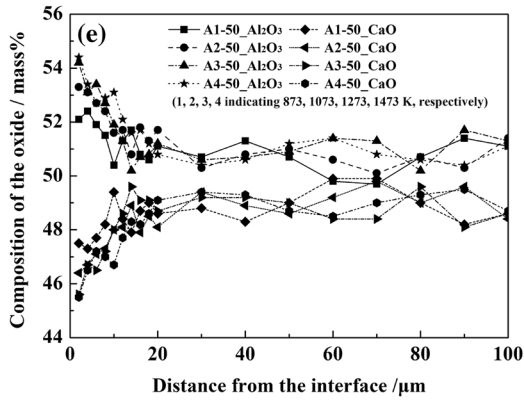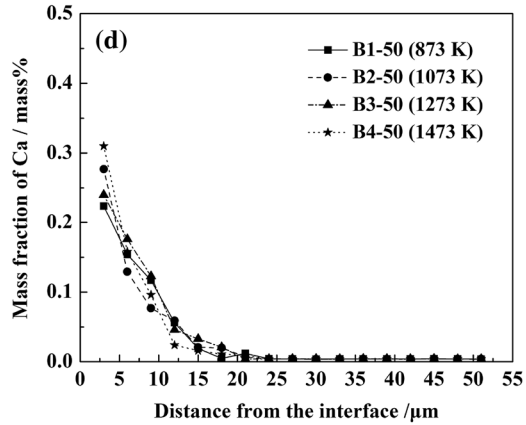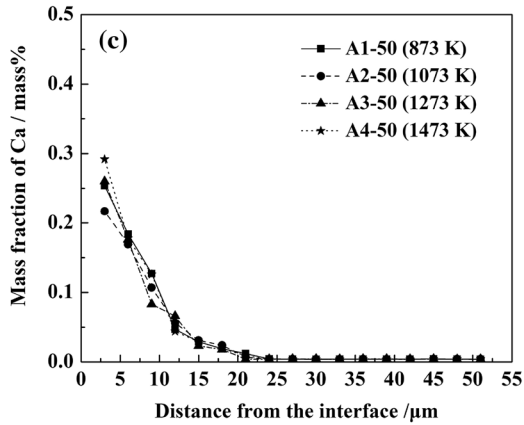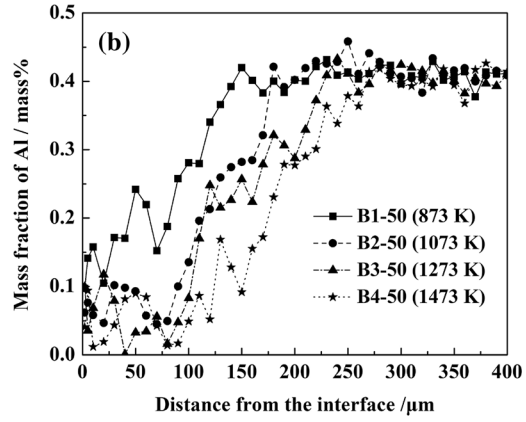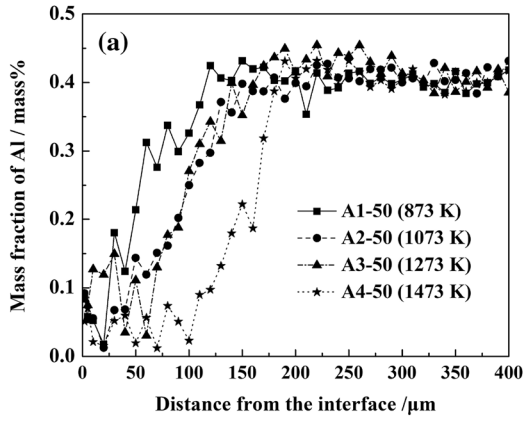
Effect of Isothermal Heating Temperature on the Interfacial Reactions Between Fe-Al-Ca Alloy and Al_2O_3-CaO-FeO Oxide

1799

width, some simplifying assumptions were made as follows:

1. The interfacial reactions completely and rapidly occur only at the reaction front.
2. The solubility of the reaction products, including the Al_2O_3 particles and $CaO \cdot Al_2O_3$ branch inclusions, are low enough to be neglected.

So, based on the Wagner equations for predicting the thickness of the internal oxidation zone,[19] a dynamic calculation model was proposed for calculating the PPZ width in the interfacial reactions between the Fe-Al-Ca alloy and the Al_2O_3-CaO-FeO oxide and is expressed as follows:

$$\xi^2 = \frac{2N_O^{(s)}D_O}{vN_B}t \tag{4}$$

where ξ indicates the PPZ width of the interfacial reaction between the alloy and the oxide; $N_O^{(s)}$ is the concentration of dissolved oxygen at the alloy–oxide interface, which is determined by the solubility of oxygen in the alloy; D_O is the diffusivity of oxygen in the alloy, which can be obtained from Eq. 5,[24] where A is the frequency factor and Q_O is the activation energy for diffusion of oxygen in γ-iron; v is the atomic ratio of oxygen to B in the precipitated inclusions, including Al_2O_3 particles and $CaO \cdot Al_2O_3$ branch inclusions; and N_B is the concentration of the alloying element. In consideration of the two reaction products, the Al_2O_3 particles and $CaO \cdot Al_2O_3$ branch inclusions, Eq. 4 was further modified and improved to precisely reflect the interfacial reactions, as show in Eq. 6:

$$D_O = A \cdot \exp\left[-\frac{Q_O}{RT}\right] \tag{5}$$

$$\xi^2 = a \cdot \frac{2N_O^{(s)}D_O}{v_{Al_2O_3}N_B}t + b \cdot \frac{2N_O^{(s)}D_O}{v_{CaO \cdot Al_2O_3}N_B}t \tag{6}$$

where a and b represent partition coefficients, which can be obtained by measuring the area proportions of the Al_2O_3 particles and $CaO \cdot Al_2O_3$ branch inclusions in the PPZ after isothermal heating using an ASPEX automatic scanning electron microscope. The values of the various parameters involved in the dynamic calculation model in this study are shown in Table II. In this table, the diffusion coefficient of oxygen in austenite is listed for each temperature. The method for calculating the concentration of dissolved oxygen at the alloy–

oxide interface, $N_O^{(s)}$, is the same as that described in previous work and is represented by Eqs. 7–9.[16,17,25,26] Figure 3 demonstrates that the FeO content in the oxide gradually decreased with increasing isothermal heating temperature. The activity coefficient of FeO was obtained by the regular solution model, as expressed in Eq. 7.[27] Oxygen partial pressure in the system and oxygen concentration in the alloy was obtained by Eqs. 8 and 9, respectively. Then combined with the experimental results shown in Fig. 3, the values of $N_O^{(s)}$ in diffusion couples A and B at different isothermal heating temperatures were calculated, and the results are listed in Table II. v was calculated by assuming the formation of pure Al_2O_3 particles and $CaO \cdot Al_2O_3$ branch inclusions wherein the ratio of elemental O to elemental B (Al and Ca) was 1.5 and 1.33, respectively, and N_B was calculated from the composition of the alloy used in this experiment:

$$RT \ln \gamma_i = \sum_j \alpha_{ij}X_j^2 + \sum_j \sum_k (\alpha_{ij} + \alpha_{ik} - \alpha_{jk})X_jX_k + I' \tag{7}$$

In this equation, i represents the activity coefficient of one component in a multicomponent regular solution; X_i is the cation fraction; α_{ij} is the interaction energy between cations; and I' is the conversion factor of the activity coefficient between a hypothetical regular solution and the real solution:
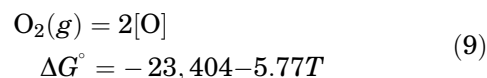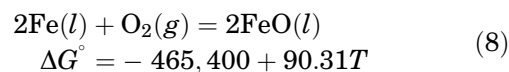
$$2Fe(l) + O_2(g) = 2FeO(l)$$
$$\Delta G^\circ = -465,400 + 90.31T \tag{8}$$

$$O_2(g) = 2[O]$$
$$\Delta G^\circ = -23,404 - 5.77T \tag{9}$$

Figure 5 depicts the relationship between the square of the PPZ width and the isothermal heating time for diffusion couples A and B based on experiments and the calculation models. Generally, the experimental results corresponded well with the calculated plots in all cases, although small deviations still existed for higher heating temperatures. The PPZ width increased with increasing isothermal heating time. For diffusion couple B, the squares of the PPZ growth kinetics at 873 K, 1073 K, 1273 K, and 1473 K all fit well to parabolic laws, while for diffusion couple A, which is affected by the precipitation of $CaO \cdot Al_2O_3$ branch inclusions, the PPZ growth trend gradually follows an exponential curve instead of the initial parabolic curve with the heating time increasing. This modified dynamic model for predicting the PPZ width contributed to understanding the interfacial reactions between the Fe-Al-Ca alloy and the Al_2O_3-CaO-FeO oxide during isothermal heating.

Interfacial reactions between the Fe-Al-Ca alloy and the Al_2O_3-CaO-FeO oxide with different FeO contents in the two diffusion couples indicate that

Effect of Isothermal Heating Temperature on the Interfacial Reactions Between Fe-Al-Ca Alloy and Al_2O_3-CaO-FeO Oxide

1801
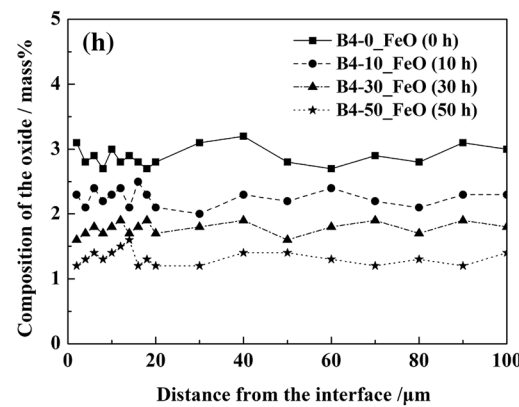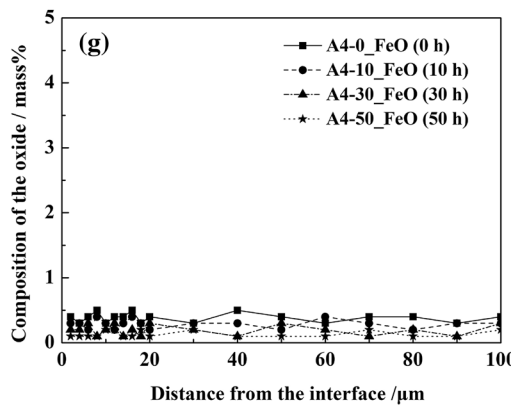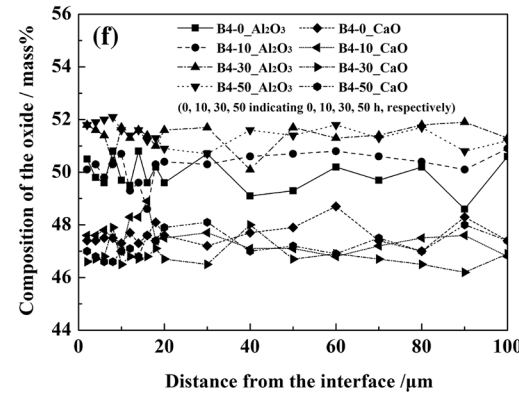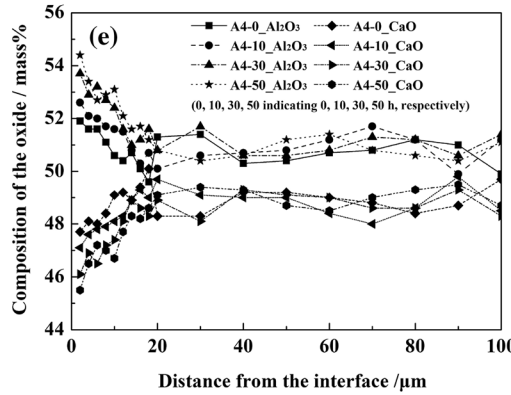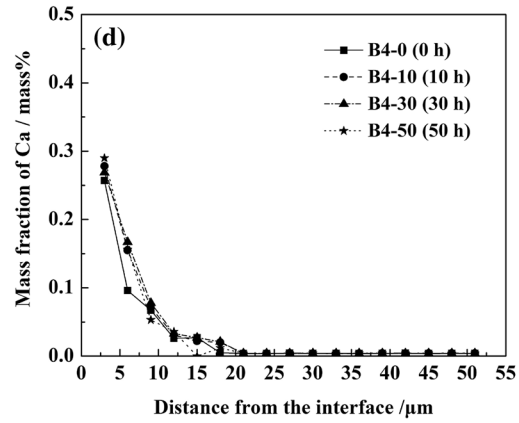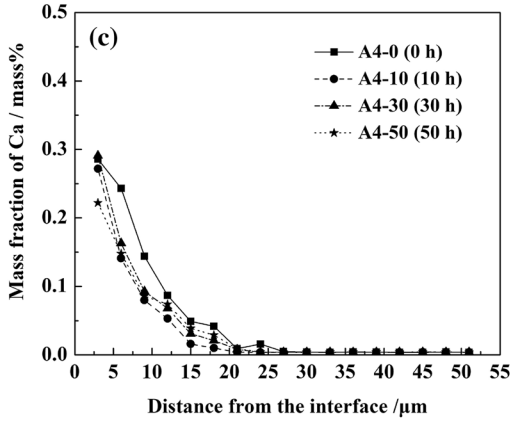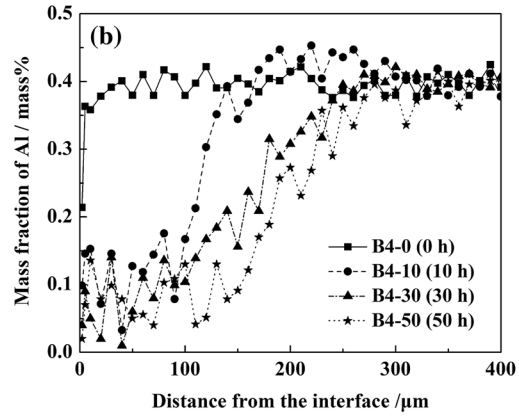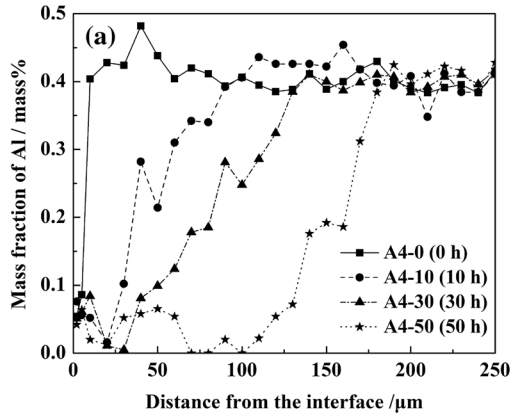
◄Fig. 3. Compositions of the alloy and oxide near the interfaces of the diffusion couples before and after isothermal heating at 1473 K: (a) Al in diffusion couple A; (b) Al in diffusion couple B; (c) Ca in diffusion couple A; (d) Ca in diffusion couple B; (e) Al_2O_3 and CaO contents in the oxide of diffusion couple A; (f) Al_2O_3 and CaO contents in the oxide of diffusion couple B; (g) FeO content in the oxide of diffusion couple A; (h) FeO content in the oxide of diffusion couple B.

the alloy and oxide are not equilibrated at those temperatures. Compared with the oxide sample used in the experiments, the actual Al_2O_3-CaO-FeO inclusion in steel is expected to be much smaller and more sensitive to the isothermal heating. Nonequilibrium between the steel and inclusion will probably lead to significant change in the composition of the inclusion after heating. Full understanding on the mechanism of the alloy–oxide interfacial reactions helps to better control the unexpected modification on the Al_2O_3-CaO-FeO inclusion due to heat treatment in practical production. In addition, due to the extremely small size of the inclusion, PPZ and ADZ widths in the steel are probably much shorter wherein the precipitated

inclusions are also expected to be much less and finer, compared with those in this study. The effects of the interfacial reactions during heating on the bond between the steel and Al_2O_3-CaO-FeO inclusion and the quality of steel product need to be further investigated during subsequent rolling or forging process.

CONCLUSION

Two diffusion couples with different FeO contents in the Al_2O_3-CaO-FeO oxide were produced and then subjected to isothermal heating at different temperatures in the range of 873 K and 1473 K for 10 h, 30 h, and 50 h. The following conclusions can be drawn from the results of this study:

1. With increasing isothermal heating temperature in the range of 873 K and 1473 K, for a low initial FeO content in the oxide (0.5 mass%), fine Al_2O_3 particles first precipitated in the alloy near the alloy–oxide interface, and then CaO·Al$_2$O$_3$ branch inclusions appeared and increased in number. For a higher initial FeO content in the oxide of 3.0 mass%, only fine Al_2O_3 particles
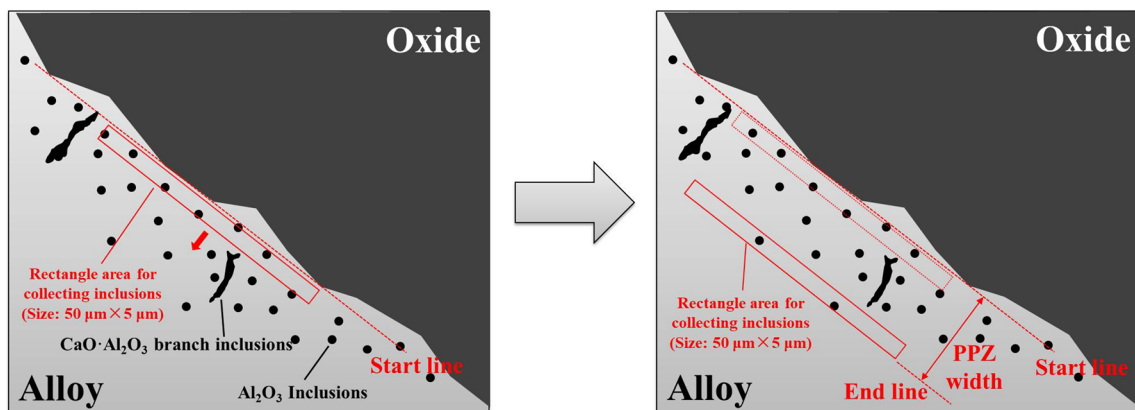

Fig. 4. Method used to define and calculate the PPZ width in the experiments.

Table II. Parameters used to calculate the PPZ width

Oxide		v			N_B
Al_2O_3		1.50			0.400
CaO·Al$_2$O$_3$		1.33			0.404

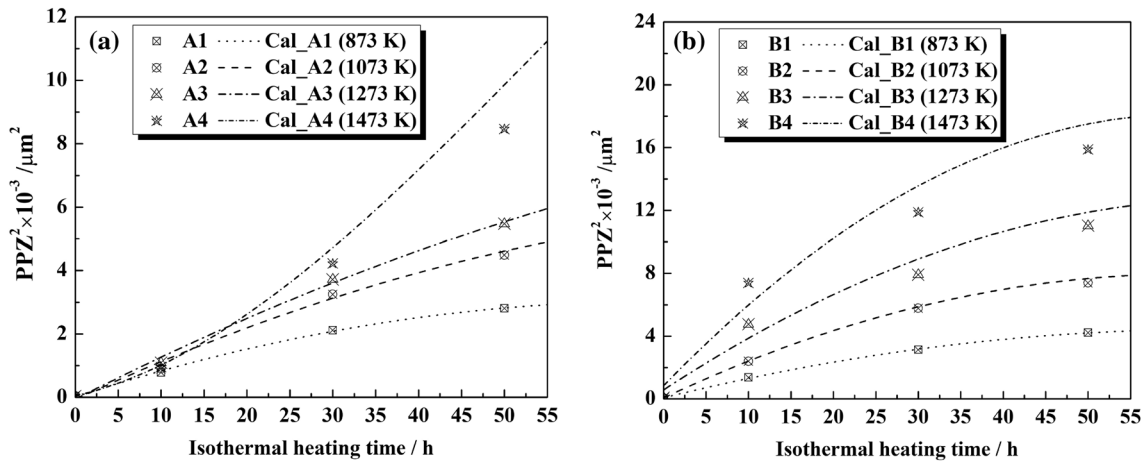| Temperature (K)	Initial FeO content in the oxide (wt.%)	$N_O^{(s)}$	D_O (cm^2 s^{-1})	a (%)	b (%)
873	0.5	1.77×10^{-9}	1.52×10^{-10}	6.2	93.8
	3.0	1.05×10^{-8}		99.6	0.4
1073	0.5	2.18×10^{-8}	1.08×10^{-8}	13.7	86.3
	3.0	1.30×10^{-7}		99.8	0.2
1273	0.5	1.22×10^{-7}	2.01×10^{-7}	41.9	58.1
	3.0	7.27×10^{-7}		100	0.0
1473	0.5	4.27×10^{-7}	1.69×10^{-6}	68.5	31.5
	3.0	2.55×10^{-6}		99.7	0.3

Fig. 5. Relationship between the square of the PPZ width and the isothermal heating time for diffusion couples based on experiments and the calculation model: (a) diffusion couples A; (b) diffusion couples B.

formed in the PPZ at each heating temperature.

2. Both PPZ and ADZ widths in the alloy–oxide diffusion couples were positively correlated to the isothermal heating time, temperature, and the initial FeO content in the oxide.

3. In consideration of the two reaction products in PPZ, Al_2O_3 particles, and $CaO \cdot Al_2O_3$ branch inclusions, a modified dynamic model for predicting the PPZ width was proposed and verified by experimental results for better understanding the interfacial reactions that occur between the alloy and the oxide during isothermal heating.

REFERENCES

1. Y.N. Wang, J. Yang, R.Z. Wang, X.L. Xin, and L.Y. Xu, *Metall. Trans. B* 47B, 1697 (2016).
2. H.T. Ling, L.F. Zhang, and H. Li, *Metall. Trans. B* 47B, 2991 (2016).
3. Z.H. Wu, W. Zheng, G.Q. Li, H. Matsuura, and F. Tsukihashi, *Metall. Trans. B* 46B, 1226 (2015).
4. I. Takahashi, T. Sakae, and T. Yoshida, *Tetsu-to-Hagané* 53, 350 (1967).
5. H. Shibata, K. Kimura, T. Tanaka, and S. Kitamura, *ISIJ Int.* 51, 1944 (2011).
6. Y. Ren, L.F. Zhang, and P.C. Pistorius, *Metall. Trans. B* 48B, 2281 (2017).
7. W. Choi, H. Matsuura, and F. Tsukihashi, *ISIJ Int.* 51, 1951 (2011).
8. K. Takano, R. Nakao, S. Fukumoto, T. Tsuchiyama, and S. Takaki, *Tetsu-to-Hagané* 89, 120 (2003).
9. H. Shibata, T. Tanaka, K. Kimura, and S. Kitamura, *Ironmak. Steelmak.* 37, 522 (2010).
10. C.S. Liu, X.Q. Liu, S.F. Yang, J.S. Li, H.W. Ni, and F. Ye, *Metals* 7, 223 (2017).
11. Y.Z. Chen, K. Wang, G.B. Shan, A.V. Ceguerra, L.K. Huang, H. Dong, L.F. Cao, S.P. Ringer, and F. Liu, *Acta Mater.* 158, 340 (2018).
12. W.Z. Mu, N. Dogan, and K.S. Coley, *Metall. Trans. B* 48B, 2379 (2017).
13. Y. Higuchi, M. Mitsuhiro, and S. Fukagawa, *ISIJ Int.* 36, S151 (1996).
14. K. Mizuno, H. Todoroki, M. Noda, and T. Tohge, *Ironmak. Steelmak.* 28, 93 (2001).
15. N. Verma, P.C. Pistorius, R.J. Fruehan, M.S. Potter, H.G. Oltmann, and E.B. Pretorius, *Metall. Trans. B* 43B, 830 (2012).
16. C.S. Liu, S.F. Yang, J.S. Li, H.W. Ni, and X.L. Zhang, *Metall. Trans. B* 48B, 1348 (2017).
17. C.S. Liu, S.F. Yang, J.S. Li, H.W. Ni, and X.L. Zhang, *Metals* 7, 129 (2017).
18. H.Y. Mu, T.S. Zhang, R.J. Fruehan, and B.A. Webler, *Metall. Trans. B* (2018). https://doi.org/10.1007/s11663-018-1294-8.
19. F. Maak, *Z. Metallk.* 52, 545 (1961).
20. C. Wagner, *Z. Elektrochem.* 63, 772 (1959).
21. G. Böhm and M. Kahlweit, *Acta Metall.* 12, 641 (1964).
22. C.S. Liu, K.H. Kim, S.J. Kim, J.S. Li, S. Ueda, X. Gao, H. Shibata, and S.Y. Kitamura, *Metall. Trans. B* 46B, 1875 (2015).
23. C.S. Liu, S.F. Yang, K.H. Kim, J.S. Li, H. Shibata, and S.Y. Kitamura, *Int. J. Miner. Metall. Mater.* 22, 811 (2015).
24. J. Takada, S. Yamamoto, S. Kikuchi, and M. Adachi, *Metall. Trans. A* 17A, 221 (1986).
25. S. Ban-ya and E. Tasuhiko, *Physical Chemistry of Metals*, 1st ed. (Tokyo: Maruzen Press, 1996), pp. 198–208.
26. E.T. Turkdogan, *Physical Chemistry of High Temperature Technology*, 1st ed. (New York: Academic Press, 1980), p. 81.
27. S. Ban-ya, *ISIJ Int.* 33, 2 (1993).